11th International Workshop on Ship and Marine Hydrodynamic
Hamburg, Germany, September 22-25, 2019

Damping of Non-Linear and Irregular Long-Crested Free-Surface Waves Using Forcing Zones

Robinson Perić[1,*], Moustafa Abdel-Maksoud[1]

[1]Hamburg University of Technology, Institute for Fluid Dynamics and Ship Theory
Am Schwarzenberg-Campus 1, 21073 Hamburg, Germany

[*]Corresponding author, robinson.peric@tuhh.de

1 ABSTRACT

Forcing-zone-type approaches (such as absorbing layers, damping zones, sponge layers, relaxation zones, etc.) can be used to reduce undesired wave reflections at the domain boundaries in flow simulations with free-surface waves. They introduce source terms in one or several of the governing equations in a zone adjacent to the corresponding domain boundaries, with the intention of gradually forcing the solution within the zone towards some reference solution. These source terms contain case-dependent parameters that require tuning. Perić and Abdel-Maksoud (2018) presented a theory which predicts the reflection coefficients and the flow within forcing zones. The present work investigates the accuracy of the theory via 2D-flow simulations with forcing zones for strongly non-linear and irregular free-surface waves. The results provide insight into the mechanisms behind how forcing zones reduce undesired wave reflections. Application of the present findings to 3D-flow simulations is discussed. When the forcing zone was tuned using the developed theory, the simulation results for reflection coefficient C_R were in most cases smaller or nearly equal to those predicted by theory, but never more than 2.1% larger. Therefore the theory is recommended for tuning forcing zones with non-linear and irregular free-surface waves.

2 INTRODUCTION

In flow simulations, it is typically desired to choose the computational domain as small as possible to reduce the computational effort. Therefore, when simulating free-surface wave propagation, undesired wave reflections at the domain boundaries must be minimized.

Forcing zones (such as absorbing layers, damping zones, sponge layers, relaxation zones, etc.) can be used to reduce such undesired wave reflections (cf. e.g. Choi and Yoon, 2009; Israeli and Orszag, 1981; Jacobsen et al., 2012; Kim et al., 2012; Park et al., 1999; Vukčević et al., 2016a, 2016b). They introduce source terms in one or several of the governing equations in a zone adjacent to the corresponding domain boundaries, with the intention of gradually forcing the solution within the zone towards some reference solution. The problem with forcing zones is to find the optimum values for their case-dependent parameters: Forcing strength γ, which regulates the magnitude of the source term, blending function $b(\mathbf{x})$, which regulates how the magnitude of the source term varies within the zone, and zone thickness x_d.

Perić and Abdel-Maksoud (2018) presented an analytical approach which predicts the reflection coefficients and the flow within forcing zones in finite-volume-based flow simulations with free-surface waves. The aim of the present work is to investigate the accuracy of their theory for strongly non-linear and irregular free-surface waves. For this, finite-volume-based flow simulations are performed with long-crested wave trains traveling towards a domain boundary, to which a forcing zone is attached to damp the waves. Simulations are performed for different parameters of the forcing zone. The resulting reflection

coefficients are compared to theory predictions.

To investigate the influence of the wave's non-linearity, flow simulations with regular deep-water waves with up to roughly 85% of the maximum wave steepness are performed. To investigate the capability of predicting reflection coefficients for irregular waves, flow simulations with a wave train based on a JONSWAP wave energy spectrum are performed under close-to-shallow water conditions.

Sections 3 and 4 describe the implementation of forcing zones, present recent findings relevant to understanding the present work and provide a brief overview of the derivation of the theory from Perić and Abdel-Maksoud (2018). Section 5 describes the setup for the flow simulations with nonlinear and irregular surface waves in Sects. 6 and 7, followed by a discussion of the present findings in Sect. 8.

3 FORCING ZONES

Forcing zones can be implemented by introducing source terms q_i and q_α in the governing equations for fluid flow

$$\frac{\mathrm{d}}{\mathrm{d}t}\int_V \rho \ \mathrm{d}V + \int_S \rho \mathbf{v}\cdot\mathbf{n} \ \mathrm{d}S = 0 \quad , \tag{1}$$

$$\frac{\mathrm{d}}{\mathrm{d}t}\int_V \rho u_i \ \mathrm{d}V + \int_S \rho u_i \mathbf{v}\cdot\mathbf{n} \ \mathrm{d}S = \int_S (\tau_{ij}\mathbf{i}_j - p\mathbf{i}_i)\cdot\mathbf{n} \ \mathrm{d}S + \int_V \rho \mathbf{g}\mathbf{i}_i \ \mathrm{d}V + \int_V \rho q_i \ \mathrm{d}V \quad , \tag{2}$$

$$\frac{\mathrm{d}}{\mathrm{d}t}\int_V \alpha \ \mathrm{d}V + \int_S \alpha \mathbf{v}\cdot\mathbf{n} \ \mathrm{d}S = \int_V q_\alpha \ \mathrm{d}V \quad , \tag{3}$$

with volume V of control volume (CV) bounded by the closed surface S, fluid velocity vector $\mathbf{v}$ with the Cartesian components u_i, unit vector $\mathbf{n}$ normal to S and pointing outwards, time t, pressure p, fluid density ρ, components τ_{ij} of the viscous stress tensor, unit vector $\mathbf{i}_j$ in direction x_j, and volume fraction α of water.

The source terms for forcing of x_i-momentum and volume fraction α are

$$q_\mathrm{i} = \gamma b(\mathbf{x})(u_{i,\mathrm{ref}} - u_i) \quad , \tag{4}$$

$$q_\alpha = \gamma b(\mathbf{x})\,(\alpha_\mathrm{ref} - \alpha) \quad , \tag{5}$$

with reference volume fraction α_ref, reference velocity component $u_{i,\mathrm{ref}}$, forcing strength γ and blending function $b(\mathbf{x})$. Forcing strength γ regulates the magnitude with which the solution at a given cell is forced towards the reference solution. The blending term $b(\mathbf{x})$ regulates how the source term varies within the zone. In the following, exponential blending is used

$$b(\mathbf{x}) = \begin{cases} \left(\frac{\mathrm{e}^{\left(\frac{x_\mathrm{d}-\tilde{x}}{x_\mathrm{d}}\right)^2}-1}{\mathrm{e}^1-1} \right) & \text{if } |\tilde{x}| \le x_\mathrm{d} \\ 0 & \text{if } |\tilde{x}| > x_\mathrm{d} \end{cases} \quad , \tag{6}$$

where $\tilde{x}$ is the smallest distance to the closest vertical domain boundary for coordinate $\mathbf{x} = (x, y, z)^\mathrm{T}$.

The rest of this section gives a brief overview over findings from previous publications (Perić and Abdel-Maksoud, 2016 & 2018) that are relevant for understanding the work in later sections.

Forcing zone thickness x_d and forcing strength γ are case-dependent and must be adjusted for each simulation. Perić and Abdel-Maksoud (2016) showed that γ and x_d scale as

$$\gamma \propto \omega, \quad x_\mathrm{d} \propto \lambda \quad , \tag{7}$$

with angular wave frequency $\omega = \frac{2\pi}{T}$, wave period T, and wavelength λ. This scaling holds for every forcing approach and can be used to take parameters γ, $b(\mathbf{x})$, and x_d from an available simulation with successful forcing and apply them properly scaled in another simulation to obtain similar forcing as before.

Figure 1 illustrates the tendency that increasing the forcing zone thickness lowers the reflection coefficient[1] for optimum γ and broadens the range of wavelengths that are successfully damped, but also increases the domain size and thus the computational effort. Further, the comparison between left and right image in Fig. 1 shows that the forcing 'behaves' differently, depending on which governing equations the source terms are applied to:

For forcing of horizontal velocities the theory predictions were rather accurate over the whole investigated range of forcing strengths γ; for regular long-crested waves in 2D-flow, Perić and Abdel-Maksoud (2018) showed that theory predictions and simulation results for the flow both outside and within the forcing zone matched closely with regard to surface elevation, velocities, and vorticity.

If forcing was applied (also) to the vertical velocities, then for some settings reflection was significantly lower than theory predicts; this occurred especially when comparatively strong forcing acted over a short distance, e.g. for too-strong forcing where most of the wave is reflected close to the entrance to the forcing zone (as in the lower image in Fig. 2). However, the theory predictions for optimum γ were still satisfactory as Fig. 1 shows. As shown in Fig. 2, for too weak forcing the reflection occurs mainly

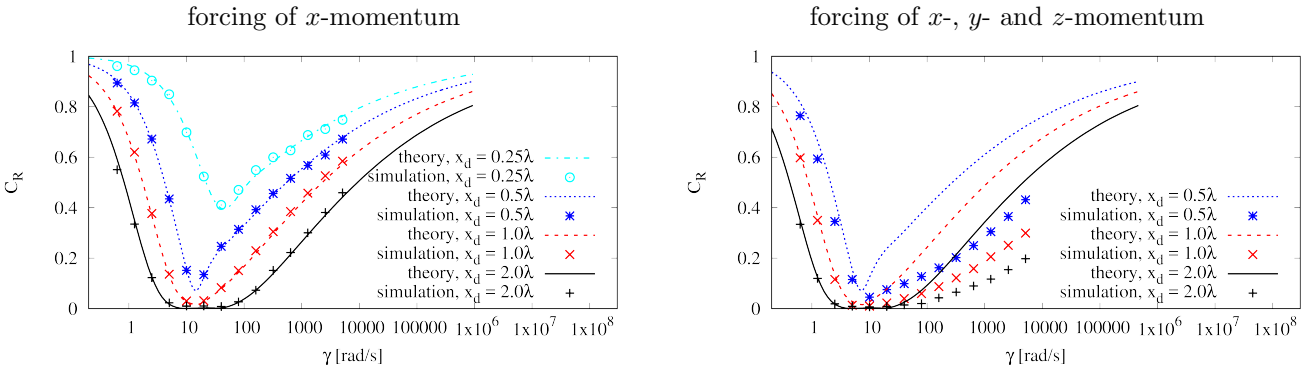

Figure 1: Reflection coefficient C_R versus forcing strength γ for different zone thicknesses x_d from 2D-flow simulations in Perić and Abdel-Maksoud (2018); for a long-crested wave with period $T = 1.6\,s$ with blending according to Eq. 6; the theory satisfactorily predicts optimum forcing strength γ

at the domain boundary to which the forcing zone is attached, while for too strong forcing the reflection occurs mainly near the entrance to the forcing zone; for optimum forcing strength the reflection occurs throughout the zone.

4 THEORY

This section gives a brief overview over the theory for predicting reflection coefficients for forcing zones; a detailed derivation can be found in Perić and Abdel-Maksoud (2018).

The theory is based on the assumption that wave reflection occurs everywhere within the forcing zone where $\nabla b(\mathbf{x}) \neq 0$. It is derived to hold with good approximation for all continuous or discontinuous blending functions $b(\mathbf{x})$. This is achieved by converting continuous blending to a piece-wise constant blending as illustrated in Fig. 3. With decreasing piece-size the theory solution was shown to converge towards the solution for continuous blending, so that for practical discretizations (> 30 cells per wavelength) the forcing zone was found to behave with good approximation discretization-independent.

Consider that long-crested waves (1D-wave propagation, 2D-flow) are generated at $x = 0$, and travel in x-direction towards boundary $x = L_x$, to which a forcing zone with thickness x_d is attached. The coordinate system origin lies at the calm water level with the z-direction pointing upwards. For

[1]The reflection coefficient $C_R = H_R/H$ is the ratio of the wave heights H_R of the reflected and H of the incidence wave.

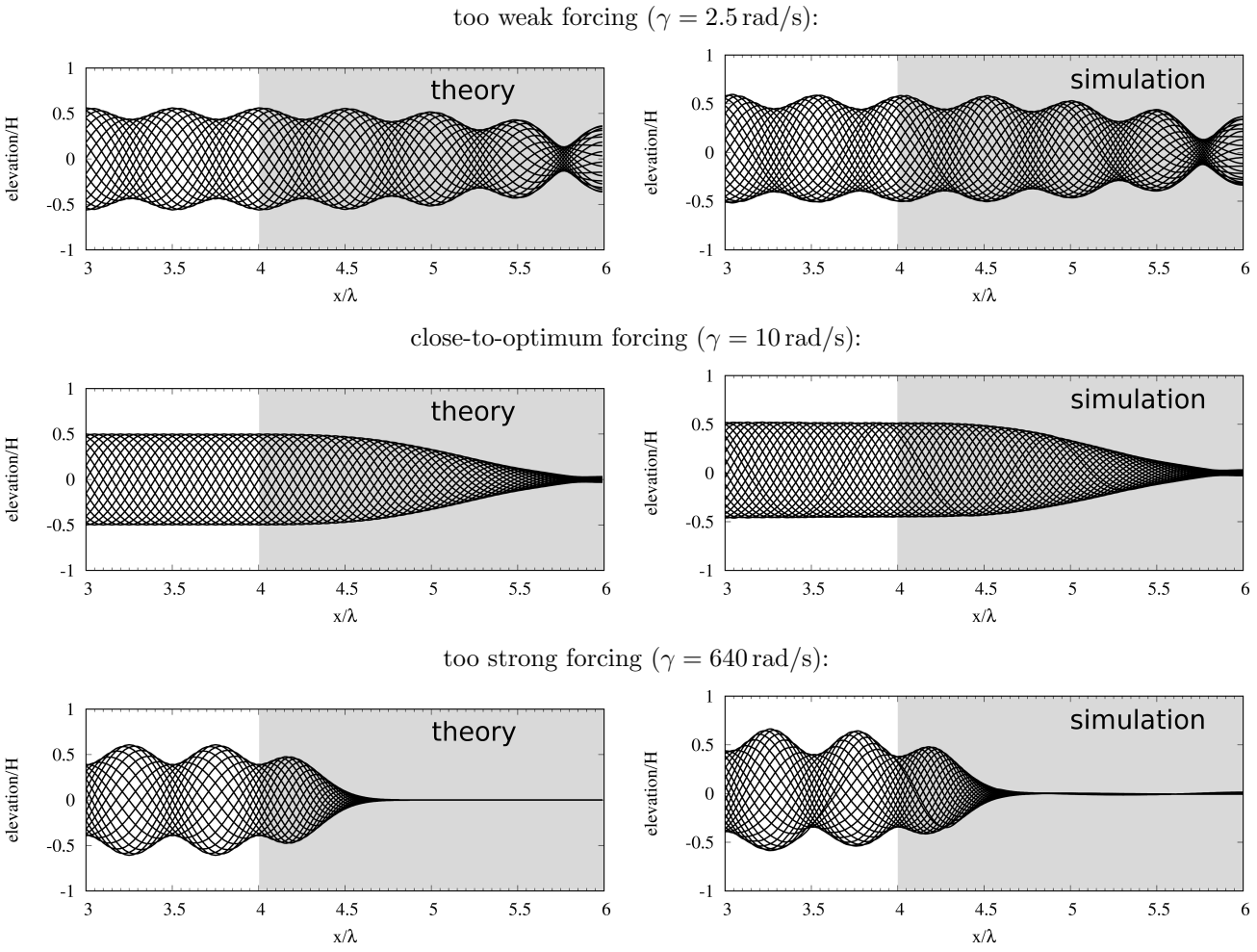

Figure 2: Theory predictions (left) and simulation results (right) for surface elevation for equally spaced time instances during the last simulated wave period $T = 1.6\,\mathrm{s}$ versus location x in wave propagation direction; wave damping using a forcing zone for x-momentum (shaded gray); the wave enters the forcing zone at $x = 16\,\mathrm{m}$; undesired wave reflections can be seen as 'bumps' in the envelope of the surface elevation (top and bottom image); 2D-flow simulation results for weakly non-linear waves (steepness ca. 29% of breaking steepness) taken from in Perić and Abdel-Maksoud (2018); the results correspond to those from the upper plot in Fig. 1 for $x_\mathrm{d} = 2\lambda$ and $\gamma = 2.5\,\mathrm{s}^{-1}, 10\,\mathrm{s}^{-1}, 640\,\mathrm{s}^{-1}$ (top to bottom)

forcing of x-momentum, the flow can then be described via the wave equation

$$\psi_{tt} = c^2\psi_{xx} + \gamma b(x)(\psi_{t,\mathrm{ref}} - \psi_t) \quad , \tag{8}$$

with velocity stream function ψ, reference solution ψ_ref, phase velocity c, forcing strength γ, and blending function $b(x)$. The last term in Eq. (8) corresponds to a forcing via Eq. (4). On each segment j of the piecewise-constant blending function $b(x)$, the wave number is constant

$$k_j = \sqrt{\frac{\omega^2 + i\omega\gamma b(\sum_{n=1}^{j-1} x_{\mathrm{d}_n} + \frac{1}{2}x_{\mathrm{d}_j})}{c^2}} \quad , \tag{9}$$

with thickness $x_{\mathrm{d},j}$ of segment j; $x_{\mathrm{d},j}$ is equivalent to the size of the segment in x-direction. Reflection and transmission may occur where $\vec{\nabla} b(\mathbf{x}) \neq 0$, i.e. at every interface between two segments.

Thus the stream function for segment $j > 0$ can be written as a sum of an incoming (propagation in positive x-direction) wave component and a reflected (propagation in negative x-direction) wave

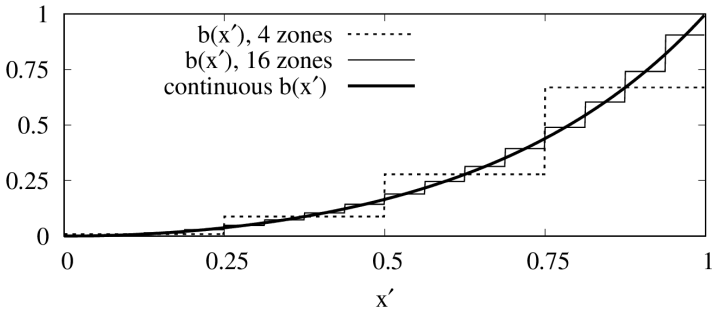

Figure 3: Blending function $b(x')$ according to Eq. (6) versus x'-coordinate; x' is directed in wave propagation direction and linearly scaled such that it is 0 at the entrance to the forcing zone and 1 at the boundary to which the zone is attached; for forcing zones consisting of 4 and 16 zones with piece-wise constant blending $b(x')$ and for continuous blending $b(x')$

component

$$\psi_j = \psi_0 \left(\prod_{n=0}^{j-1} C_{\mathrm{T}_n} \right) \cdot \left[\mathrm{e}^{i\left(\sum_{n=1}^{j-1} k_n x_{\mathrm{d}_n} + k_j \left(x - \sum_{n=1}^{j-1} x_{\mathrm{d}_n}\right)\right)} - C_{\mathrm{R}_j} \mathrm{e}^{i\left(\sum_{n=1}^{j-1} k_n x_{\mathrm{d}_n} + k_j 2x_{\mathrm{d}_j} - k_j \left(x - \sum_{n=1}^{j-1} x_{\mathrm{d}_n}\right)\right)} \right] \quad , \tag{10}$$

with the stream function for the originally generated wave at $x = 0$ being, for example according to linear wave theory,

$$\psi_0 = \frac{H\omega}{2k_0} \frac{\sinh(k_0(z+h))}{\sinh(k_0 h)} \mathrm{e}^{i(-\omega t)} \quad , \tag{11}$$

with wave height H, angular wave frequency ω, wave number k_0, vertical coordinate z, and time t.

Set the transmission coefficient $C_{\mathrm{T}_0} = 1$ and the reflection coefficient $C_{\mathrm{R}_0} = 0$, so that no reflection occurs at the 'inlet' boundary. For N zones, set $C_{\mathrm{T}_N} = 0$ and $C_{\mathrm{R}_N} = 1$ to obtain a fully reflective boundary at $x = L_x$.

By requiring that the particle displacements and velocities must be continuous at every interface between two zones, the transmission C_{T_j} and reflection C_{R_j} coefficients are obtained as

$$C_{\mathrm{T}_j} = \frac{1 - C_{\mathrm{R}_j}}{1 - C_{\mathrm{R}_{j+1}} \mathrm{e}^{i\left(k_{j+1} 2x_{\mathrm{d}_{j+1}}\right)}} \quad , \tag{12}$$

$$C_{\mathrm{R}_j} = \frac{k_{j+1}\beta_{j+1} - k_j}{k_{j+1}\beta_{j+1} + k_j} \quad , \tag{13}$$

with

$$\beta_{j+1} = \frac{1 + C_{\mathrm{R}_{j+1}} \mathrm{e}^{i\left(k_{j+1} 2x_{\mathrm{d}_{j+1}}\right)}}{1 - C_{\mathrm{R}_{j+1}} \mathrm{e}^{i\left(k_{j+1} 2x_{\mathrm{d}_{j+1}}\right)}} \quad . \tag{14}$$

For practical purposes, mainly the 'global' reflection coefficient C_{R} is of interest, which is the ratio of the amplitude of the wave that is reflected back into the solution domain, to the amplitude of the wave that enters the forcing zone. If the forcing zone starts at segment 1, then

$$C_{\mathrm{R}} = |C_{\mathrm{R}_1}| = \sqrt{\mathrm{Re}\{C_{\mathrm{R}_1}\}^2 + \mathrm{Im}\{C_{\mathrm{R}_1}\}^2} \quad , \tag{15}$$

where $\mathrm{Re}\{X\}$ and $\mathrm{Im}\{X\}$ denote the real and the imaginary part of the complex number X.

The theory for forcing of x-momentum can be extended to forcing of x-, y-, and z-momentum and volume fraction α. For this, assume that applying forcing in one governing equation acts instantly on the other governing equations and relate the forcing strength γ to the wave energy components associated with the governing equations to which the source terms are applied. For example, forcing of volume fraction α, x-, y-, and z-momentum with a forcing strength $\gamma_{\alpha xyz}$ is equivalent to forcing of x-momentum with forcing strength γ, when holds

$$\gamma_{\alpha xyz} = \left(\frac{\bar{E}_{\mathrm{kin},x}}{\bar{E}_{\mathrm{kin},x} + \bar{E}_{\mathrm{kin},y} + \bar{E}_{\mathrm{kin},z} + \bar{E}_{\mathrm{pot}}} \right) \gamma \quad , \tag{16}$$

with mean kinetic wave energy components $\bar{E}_{\mathrm{kin},x}$, $\bar{E}_{\mathrm{kin},y}$ and $\bar{E}_{\mathrm{kin},z}$ in x-, y- and z-direction and mean potential wave energy $\bar{E}_{\mathrm{pot}}$; thus for deep-water conditions holds $\gamma_{\alpha xyz} = 0.25\gamma$.

A computer program for predicting the forcing zone behavior based on the above theory by Perić and Abdel-Maksoud (2018) is publicly available as free software. The code evaluates the theory for the case of long-crested waves (1D-wave propagation). The source code and manual can be downloaded from: `https://github.com/wave-absorbing-layers/absorbing-layer-for-free-surface-waves`

Relaxation zones (e.g. Chen et al., 2006; Jacobsen et al., 2012; Mayer et al., 1998; Vukčević et al., 2016) are a special case of forcing zones, in which the governing equations are faded-out when the source terms are blended-in. They can be reformulated as forcing zones as demonstrated in Perić et al. (2018), where the theory from Perić and Abdel-Maksoud (2018) was extended so that it can be used to tune the case-dependent parameters of relaxation zones; an open-source program to evaluate the theory was published along with their paper and is available for download under: `https://github.com/wave-absorbing-layers/relaxation-zones-for-free-surface-waves`

Perić (2017) demonstrated how the theory can be extended to cover oblique wave incidence in 3D-flows. The extended theory was validated using flow simulations with (hydro-)acoustic waves, and application to free-surface waves is straightforward. The extended theory was found to predict with satisfactory accuracy reflection coefficients for oblique waves depending on their incidence angle. The findings in Perić (2017) indicate that the above discussed theory's predictions (1D-wave propagation, Eqs. (8) to (16)) can be considered as an upper-boundary for the overall reflection coefficient in the 3D-flow simulation; thus the investigation of 2D-flows in the present work has practical relevance for 3D-flow simulations as well. Further research on this matter is currently in progress.

5 SIMULATION SETUP

The commercial flow solver STAR-CCM+ version 11.06.010-R8 from Siemens (formerly CD-adapco) is used for the simulations. The governing equations, Eqs. (1) to (3), are discretized according to the finite volume method. The volume of fluid (VOF) method is used to account for the two fluid phases, liquid water and gaseous air, using the High Resolution Interface Capturing scheme (HRIC) as given in Muzaferija and Perić (1999). All approximations in the discretization are of second order. The resulting coupled equation system is linearized and solved by the iterative STAR-CCM+ implicit unsteady segregated solver, using an algebraic multigrid method with Gauss-Seidel relaxation scheme, V-cycles for pressure and volume fraction of water, and flexible cycles for velocity calculation. The under-relaxation factor is 0.9 for velocities and volume fraction and 0.4 for pressure. For each time step, eight iterations are performed; one iteration consists of solving the governing equations for the velocity components, the pressure-correction equation (using the SIMPLE method for collocated grids to obtain the pressure values and to correct the velocities) and the transport equation for the volume fraction of water. Further information on the discretization of and solvers for the governing equations can be found in Ferziger and Perić (2002) or the STAR-CCM+ software manual.

Long-crested free-surface waves are generated and travel in positive x-direction towards a forcing zone as sketched in Fig. 4, where they are partly reflected and partly absorbed. The coordinate system lies at the calm free-surface level on the inlet boundary as shown in Fig. 4. The simulations are performed

quasi-2D, i.e. with only one layer of cells in y-direction and symmetry boundary conditions applied to the y-normal boundaries.

The forcing approaches from Sect. 3 are used to minimize wave reflections. Simulations are either performed with forcing of x-momentum (q_x), of z-momentum (q_z), of both x- and z-momentum (q_x, q_z), or of volume fraction α and x- and z-momentum (q_α, q_x, q_z) via Eqs. (4) and (5). The forcing zone has exponential blending according to Eq. (6) and the solution is forced towards the calm-surface solution (i.e. reference velocity $\mathbf{v}_\mathrm{ref} = (0,0,0)^\mathrm{T}$, reference volume fraction $\alpha_\mathrm{ref} = 1$ for $z \leq 0$ and $\alpha_\mathrm{ref} = 0$ for $z > 0$). Forcing zone thicknesses x_d in the range between 1λ and 2λ are investigated.

The wave is generated by prescribing the volume fraction and velocities at the inlet boundary ($x = 0$). At the outlet boundary ($x = L_x$), the hydrostatic solution for the pressure and volume fraction for the calm-surface solution are prescribed. All remaining boundaries are no-slip walls. For further details on boundary conditions, see Ferziger and Perić (2002).

The domain is discretized using a rectilinear grid with local mesh refinement in the vicinity of the free surface.

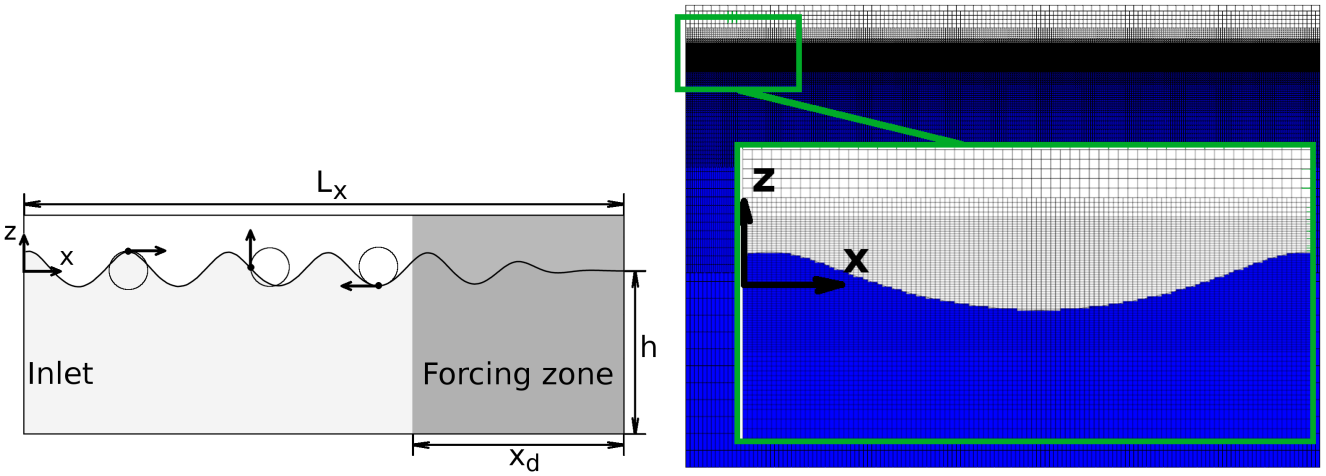

Figure 4: Left: 2D-Simulation domain with forcing zone (shaded gray) of thickness x_d for damping of long-crested waves in water depth h; right: computational grid with close-up and cells containing the liquid phase colored in blue

In Sect. 6, flow simulations with regular waves in deep-water conditions ($h \geq 0.5\lambda$) are performed, with wave period $T = 1.6\,\mathrm{s}$ and thus wavelength $\lambda \approx 4\,\mathrm{m}$. Different wave heights H are investigated to study the influence of the wave's non-linearity on the forcing zone behavior. The domain has dimensions $0 \leq x \leq L_x$ and $-h \leq z \leq 0.5\lambda$, with domain length $L_x = 6\lambda$ and water depth $h = 4.5\lambda$. The local mesh refinement extended so far from the calm-surface level that the same grid could be used for all simulations. The free-surface was discretized by > 100 cells per wavelength and > 14 cells per wave height. The time-step was $\Delta t = T/570$ in terms of wave period T. The forcing zone had exponential blending according to Eq. (6) and a zone thickness of $x_\mathrm{d} = 2\lambda_0$. Fenton's (1985) 5^th-order Stokes theory is used to initialize the flow within the domain and to generate the waves at the inlet boundary. All simulations were repeated with boundary $x = L_x$ set to wall boundary condition (results from these simulations are shown in Fig. 5) and the difference in the results was found to be negligible. The free surface stays at all times within the region of the finest mesh. The computational grid, which consists of $\approx 43\,000$ cells, is shown in Fig. 4. The total simulated time is $18\,\mathrm{s} \approx 11.3T$. The reflection coefficient C_R is calculated via Eq. (17).

To calculate reflection coefficient C_R for the regular free-surface waves, the surface elevation in the whole domain is recorded at a sufficient number (say 80) of evenly spaced time intervals during the last simulated wave period. The evaluation interval contains all cells outside the forcing zone which are within a distance of slightly more than one wavelength to the forcing zone. The overall highest and lowest wave heights recorded in this interval are determined as H_max and H_min. The domain size and simulation

duration was chosen so that wave reflections were fully developed in the evaluation interval, while possible wave re-reflections (e.g. at the inlet boundary) had not yet traveled back into the evaluation interval. The reflection coefficient is calculated as in Ursell et al. (1960) via

$$C_{\mathrm{R}} = \left(H_{\max} - H_{\min}\right) / \left(H_{\max} + H_{\min}\right) \quad . \tag{17}$$

In Sect. 7, flow simulations with irregular waves are performed. The domain has dimensions $0 \leq x \leq L_x = 400\,\mathrm{m}$ and $-h \leq z \leq 0.5\,\mathrm{m}$ with water depth $h = 1\,\mathrm{m}$. Initially velocities u_i and volume fraction α are prescribed according to the solution for the calm free-surface. At the inlet boundary ($x = 0$), velocities u_i and volume fraction α are prescribed according to linear wave theory to generate the irregular wave train. Waves are generated during the first 60 s of simulated time, using the analytical solution for a JONSWAP wave energy spectrum (see e.g. DNV, 2014; Hasselmann et al., 1973) discretized into 300 wave components, to obtain a peak period $T_{\mathrm{peak}} = 12.82\,\mathrm{s}$, significant wave height $H_{\mathrm{s}} \approx 0.056\,\mathrm{m}$, peak wavelength λ_{peak} and peak-shape parameter 3.3. When the simulation ends at $t_{\mathrm{end}} = 220\,\mathrm{s}$, the whole wave train has encountered the forcing zone once. The free-surface is discretized with cell sizes $\Delta x = 0.625\,\mathrm{m} \approx \lambda_{\mathrm{peak}}/64$ and $\Delta z = 0.0098\,\mathrm{m} \approx H_{\mathrm{s}}/6$. The grid consists of $\approx 40\,000$ cells. The time-step is $\Delta t = 0.012823\,\mathrm{s} \approx T_{\mathrm{peak}}/1000$. Per time-step, 10 iterations are performed. Simulations are performed for different forcing zone thickness x_{d}, different forcing strength γ and with source terms applied in different governing equations.

After each simulation, the surface elevation in the whole domain is written to a file and a fast Fourier Transform (FFT) is performed on the recording to obtain the amplitudes and frequencies of the wave components. For the simulation results, the overall reflection coefficient C_{R} is then computed from the FFT results for the given forcing strength γ in relation to the FFT results for the case of $\gamma = 0$ via

$$C_{\mathrm{R}} = \frac{\sum_{n=1}^{N} a_n \Delta f_n|_{\gamma}}{\sum_{n=1}^{N} a_n \Delta f_n|_{\gamma=0}} \quad , \tag{18}$$

with the total number of frequencies N, Fourier amplitude a_n of the wave component with frequency f_n, and frequency interval $\Delta f_n = f_n - f_{n-1}$.

The theory prediction of the overall reflection coefficient C_{R} is obtained via Eq. (18) by inserting $a_n|_{\gamma} \approx C_{\mathrm{R},n} a_n|_{\gamma=0}$, with amplitude $a_n|_{\gamma=0}$ obtained for the simulation results for the case without forcing, and the corresponding reflection coefficient $C_{\mathrm{R},n}$ for each wave component n is obtained from the 1D-theory from Sect. 4. The underlying assumption is that the FFT-results can be treated as a linear superposition of waves so that the theory from Sect. 4 can be applied to each wave component separately.

For most wave components hold shallow-water conditions ($h \leq 0.05\lambda$), or else intermediate-water conditions ($0.05\lambda < h < 0.5\lambda$) which are sufficiently close to shallow water so that the wave propagation shows only comparatively small dispersion; for example, for wavelengths between $0.25\lambda_{\mathrm{peak}}$ and $4\lambda_{\mathrm{peak}}$, phase velocity c varies by $\lesssim 6\%$ according to linear wave theory. Therefore, although the wave train will change its shape during propagation, it will remain relatively compact since the relevant wave components travel at similar speeds, so that Eq. (18) is suitable for computing the reflection coefficient.

6 RESULTS FOR FORCING OF STEEP FREE-SURFACE WAVES

This section investigates the applicability of the theory from Sect. 4 to forcing of non-linear free-surface waves in deep water. Simulations were performed with different wave height H ranging from 50% to 85% of the breaking wave height H_{break} according to Michell (1893). For better comparability, the following approximation will be used $H_{\mathrm{break}} = 0.142\lambda_0 = 0.589\,\mathrm{m}$, where λ_0 is the wavelength according to linear wave theory. Steeper waves were not generated since Stokes 5^{th}-order theory was used to initialize and generate the waves; close to breaking steepness, the theory becomes inaccurate and thus introduces disturbances that can trigger wave breaking, after which a calculation of reflection coefficient C_{R} was not considered feasible[2]. Note that reflection coefficients below $1\% \lesssim C_{\mathrm{R}}$ could not be detected, since

[2]In the simulations presented in this section, slight wave breaking occurred only in a few simulations for $H \geq 0.8H_{\mathrm{break}}$ and for γ-values significantly smaller ($\gamma \lesssim \mathcal{O}(1\,\mathrm{s}^{-1})$) or larger ($\gamma \gtrsim \mathcal{O}(10^3\,\mathrm{s}^{-1})$) than optimum; these values can differ noticeably

the interface-capturing and -sharpening scheme produces a slight background-noise of the approach to calculate C_{R}.

Figure 5 demonstrates that, as with linear waves (cf. Fig. 2), for too weak forcing the wave reflection occurs mainly at the domain boundary (here: $x = 24\,\mathrm{m}$), for too strong forcing the wave reflection occurs mainly near the entrance to the forcing zone (here: $16\,\mathrm{m} \leq x \leq 18\,\mathrm{m}$), whereas for close-to-optimum forcing the wave reflection occurs more evenly throughout the whole forcing zone.

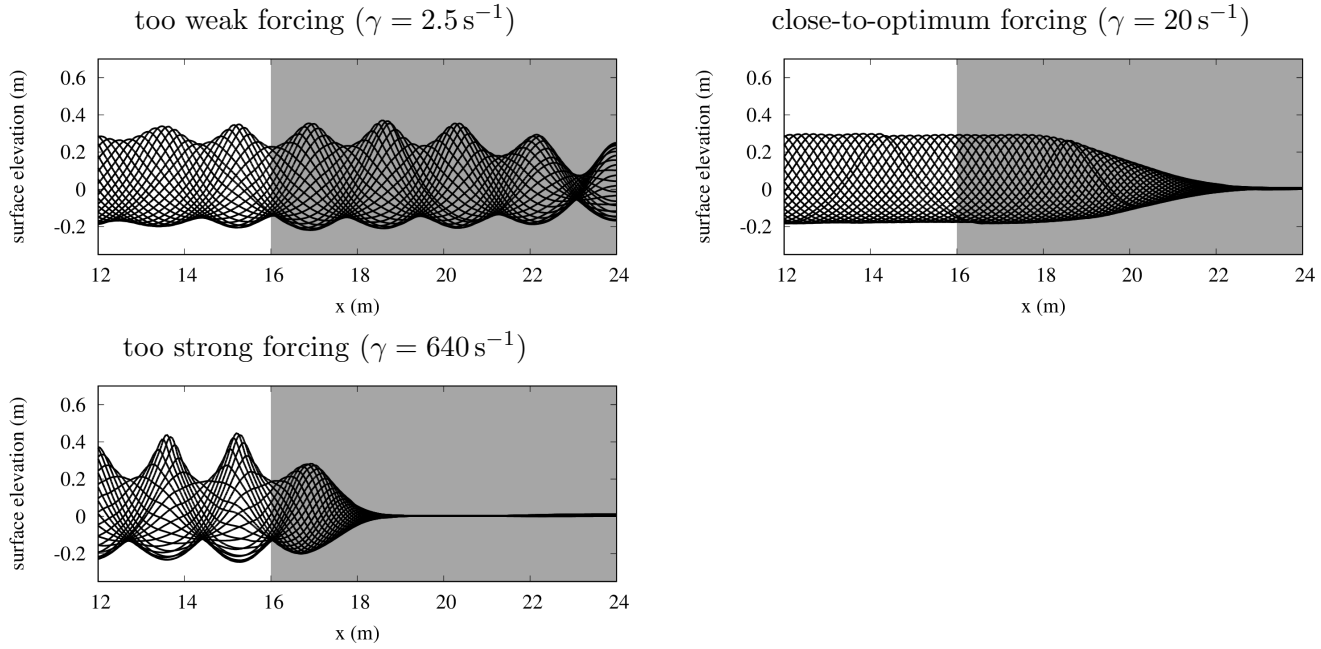

Figure 5: Simulation results for surface elevation over x-coordinate in the vicinity of the forcing zone (shaded gray), evaluated for equally spaced time intervals during the last simulated period; for the waves from Fig. 6 with height $H \approx 0.85 H_{\mathrm{break}}$ relative to breaking wave height H_{break}

Figures 5 and 6 show that the wave steepness – and thus also the wave's non-linearity – has a negligible influence on the results for reflection coefficient C_{R}. Therefore the theory is also recommended for tuning forcing zones in the presence of non-linear free-surface waves.

Figure 7 shows that the theory also applies to forcing of all velocities u_i and volume fraction α. Although for too strong forcing the theory over-predicts C_{R}, the optimum values for the case-dependent parameters of the forcing zone are predicted reasonably well as before.

7 RESULTS FOR FORCING OF IRREGULAR FREE-SURFACE WAVES

This section investigates to which extent the theory from Sect. 4 is suitable for predicting reflection coefficients for forcing zones with irregular free-surface waves.

Figures 8 to 10 show that, for a forcing zone thickness of $x_{\mathrm{d}} \approx 1\lambda_{\mathrm{peak}} \approx 40\,\mathrm{m}$ and forcing of velocity u towards $u_{\mathrm{ref}} = 0$, the theory predictions and simulation results for reflection coefficient C_{R} show satisfactory agreement. Further, Fig. 10 shows that 1D-theory for a regular wave with period $T = T_{\mathrm{peak}}$ can be used to tune the forcing zone: the optimum value for γ is reasonably well predicted, although the reflection coefficient is under-predicted; thus when tuning only according to the peak period, thicker forcing zones should be used to ensure that the desired reflection coefficient is obtained.

Repeating the simulations from Figs. 8 to 10 with only forcing of volume fraction α, the results in

in reflection coefficient compared to the other simulation results.

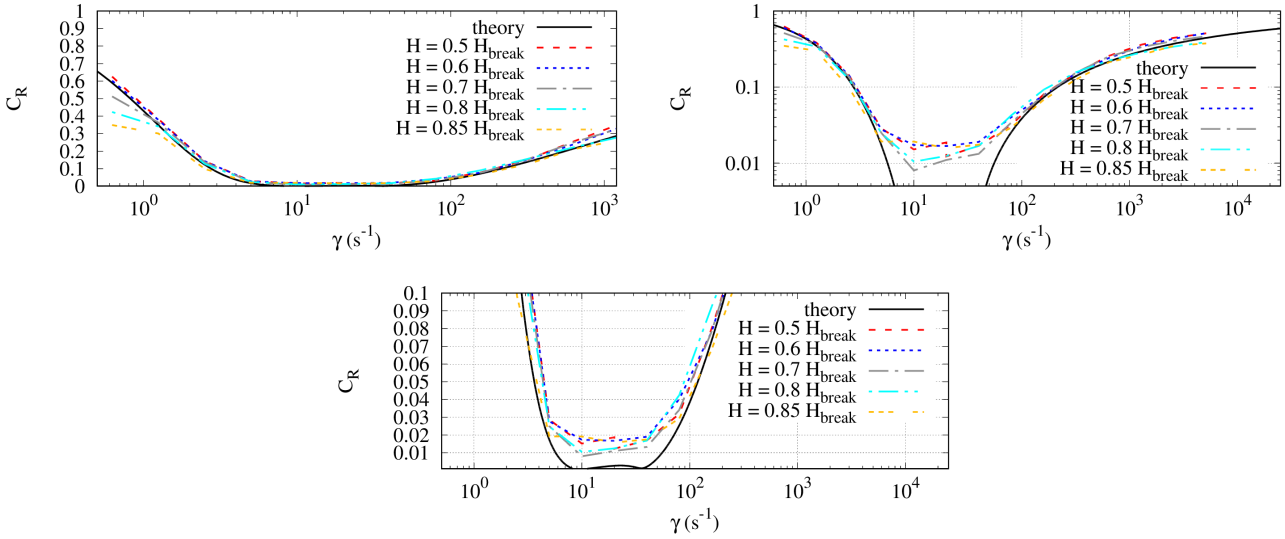

Figure 6: Reflection coefficient C_R over forcing strength γ for different wave heights H relative to wave breaking height H_break, according to simulation results and theory prediction; results are shown with logarithmic y-axis (top, right) and for a close-up (bottom); for deep-water waves with period $T = 1.6\,\mathrm{s}$; for blending according to Eq. (6), zone thickness $x_\mathrm{d} = 2\lambda_0$, and forcing of x-momentum towards $u_\mathrm{ref} = 0$; for all simulation results $C_\mathrm{R,sim}$ and corresponding theory predictions $C_\mathrm{R,theory}$ holds $C_\mathrm{R,sim} - C_\mathrm{R,theory} < 7.4\%$ and on average $|C_\mathrm{R,sim} - C_\mathrm{R,theory}| < 3.1\%$; for the forcing strength $\gamma \geq \gamma_\mathrm{opt,theory}$ closest to the theoretical optimum value $\gamma_\mathrm{opt,theory}$ holds $C_\mathrm{R,sim} - C_\mathrm{R,theory} < 1.9\%$

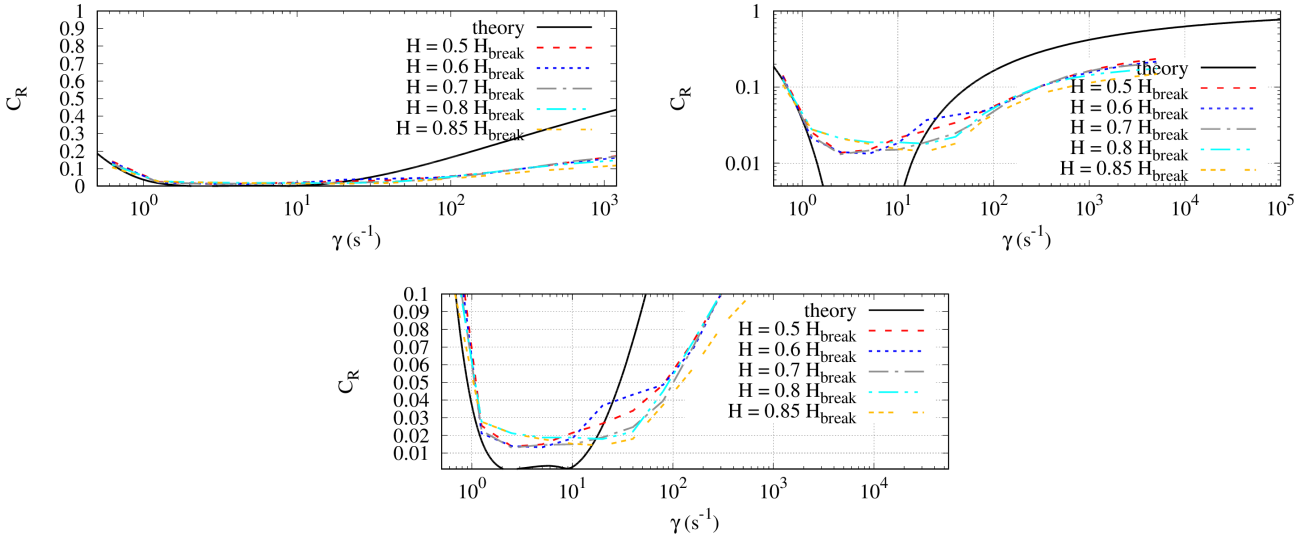

Figure 7: As Fig. 6, except for forcing of x- and z-momentum as well as volume fraction α towards the calm-surface solution; for all simulation results $C_\mathrm{R,sim}$ and corresponding theory predictions $C_\mathrm{R,theory}$ holds $C_\mathrm{R,sim} - C_\mathrm{R,theory} < 2.1\%$; for the forcing strength $\gamma \geq \gamma_\mathrm{opt,theory}$ closest to the theoretical optimum value $\gamma_\mathrm{opt,theory}$ holds $C_\mathrm{R,sim} - C_\mathrm{R,theory} < 2.1\%$

Figs. 11 to 13 are remarkably similar to those obtained for forcing of x-momentum.

Repeating the simulations from Figs. 8 to 10 with only forcing of z-momentum, the results in

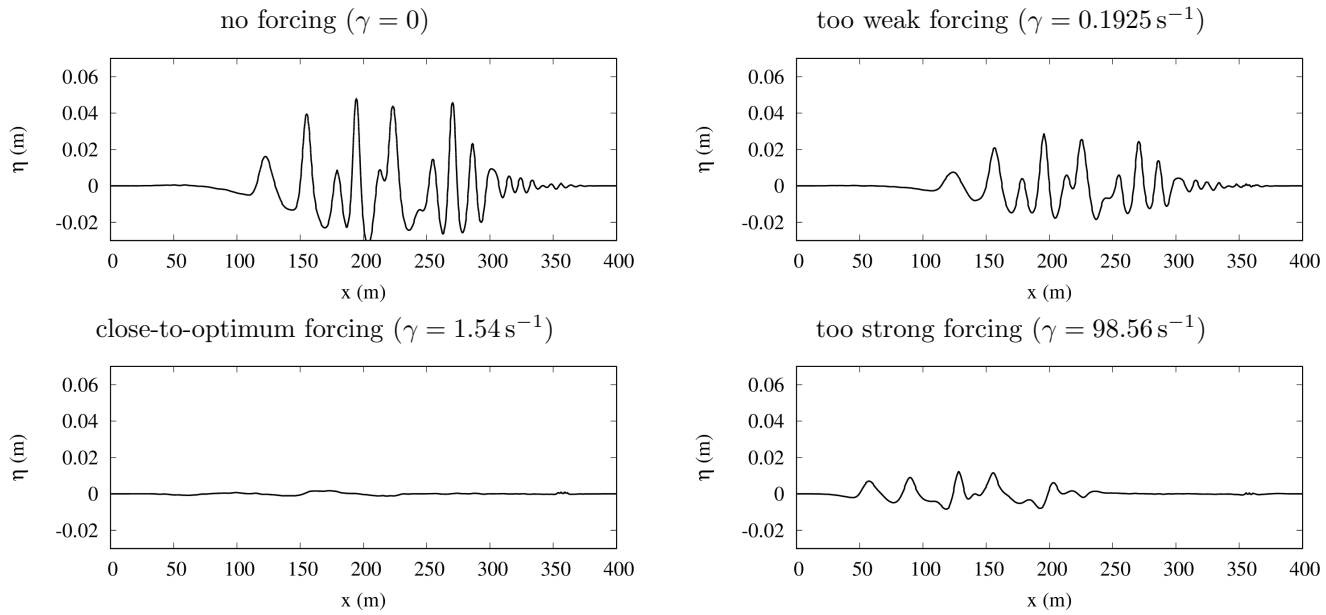

Figure 8: Surface elevation over x-location at time $t = 220\,\mathrm{s}$; for irregular waves with peak period $T_{\mathrm{peak}} = 12.82\,\mathrm{s}$ in intermediate to shallow water; for forcing of x-momentum with blending via Eq. (6) and zone thickness $x_{\mathrm{d}} \approx 1\lambda_{\mathrm{peak}}$

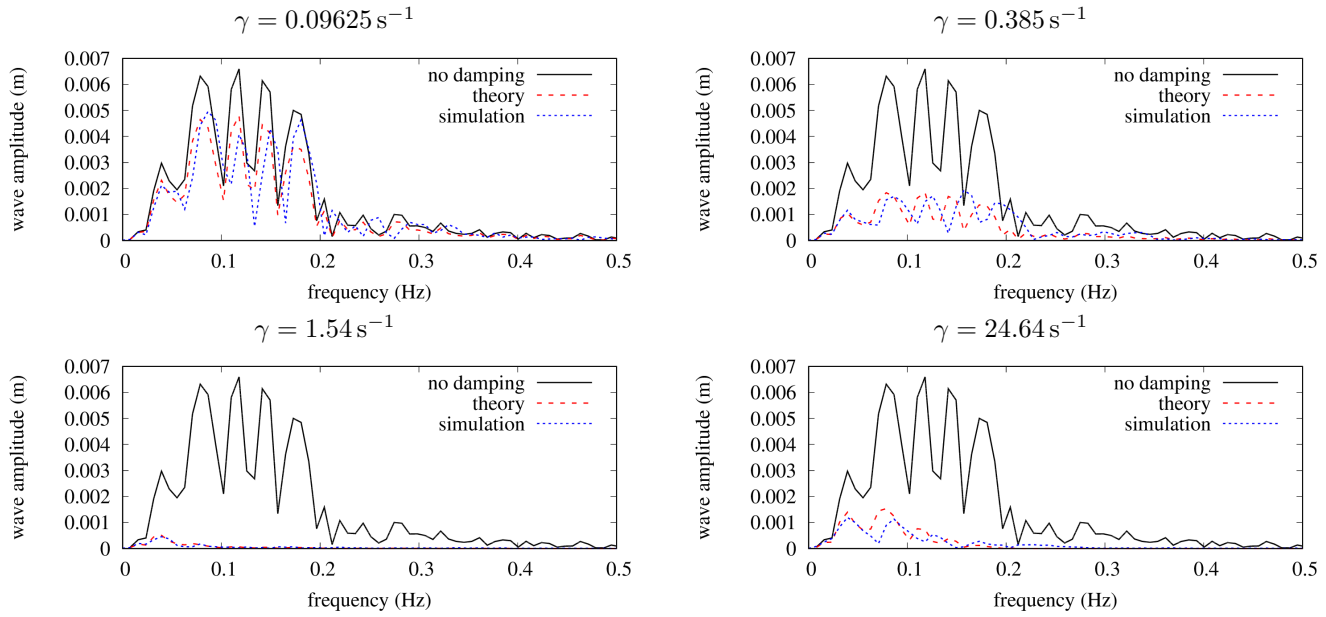

Figure 9: Wave amplitude a_n over frequency f_n, obtained from FFT of the surface elevation at time $t = 220\,\mathrm{s}$ as in Fig. 8; simulation results for no damping ($\gamma = 0$) and for forcing strength γ, as well the theory prediction; for irregular waves with peak period $T_{\mathrm{peak}} = 12.82\,\mathrm{s}$ in intermediate to shallow water; for forcing of x-momentum with exponential blending via Eq. (6) and zone thickness $x_{\mathrm{d}} \approx 1\lambda_{\mathrm{peak}}$

Fig. 14 differ considerably from those obtained for forcing of x-momentum: The optimum value fo γ is two orders of magnitude larger. This was expected, since linear wave theory shows that the vertical component of the kinetic energy is two orders of magnitude smaller than the horizontal kinetic energy due to the limited water depth. Since the forcing acts on the vertical kinetic energy, a significantly larger forcing strength is therefore required as outlined in Sect. 4.

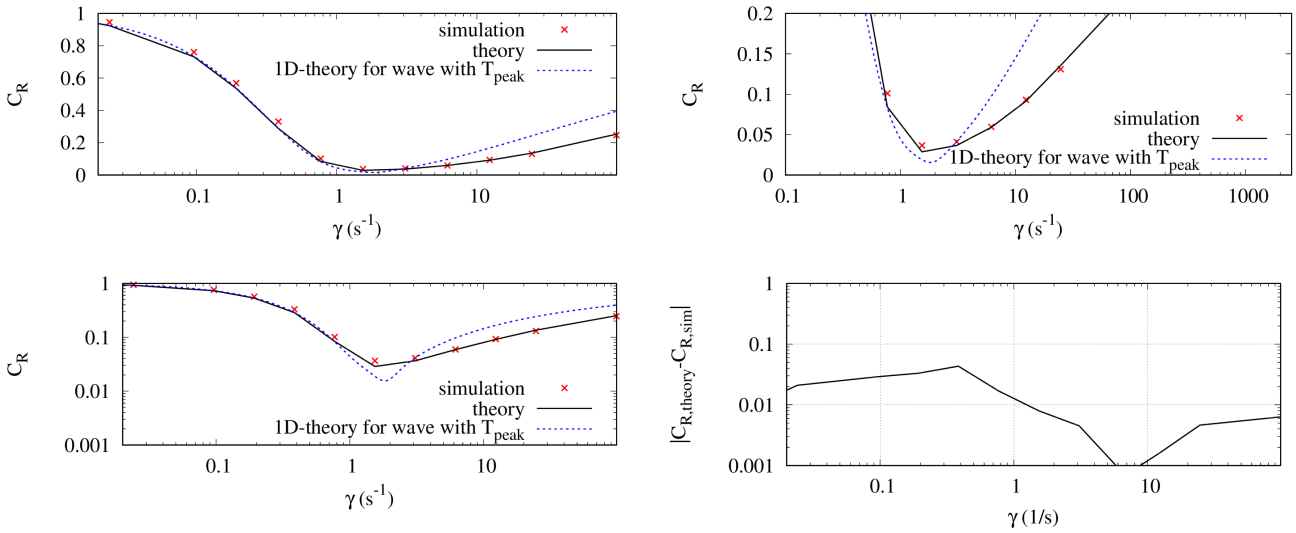

Figure 10: Top left, top right, bottom left: Overall reflection coefficient C_R for damping of the irregular wave train from Fig. 9 over forcing strength γ, from theory prediction and simulation results; for forcing of x-momentum with exponential blending via Eq. (6) and zone thickness $x_\mathrm{d} \approx 1\lambda_\mathrm{peak}$; for all simulation results $C_\mathrm{R,sim}$ and corresponding theory predictions $C_\mathrm{R,theory}$ holds $C_\mathrm{R,sim} - C_\mathrm{R,theory} < 4.4\%$ and on average $|C_\mathrm{R,sim} - C_\mathrm{R,theory}| < 1.3\%$; for the forcing strength $\gamma \geq \gamma_\mathrm{opt,theory}$ closest to the theoretical optimum value $\gamma_\mathrm{opt,theory}$ holds $C_\mathrm{R,sim} - C_\mathrm{R,theory} < 0.8\%$; the curve for 1D-theory for a monochromatic wave with T_peak shows that tuning the forcing zone for the peak period gives a satisfactory guess at the optimum choice of γ; bottom right: absolute difference between theory prediction and simulation results for C_R over γ

Figure 14 further shows that for too weak forcing the theory overpredicts reflection coefficient C_R. In the extension of the theory for applying forcing source terms in different governing equations in Sect. 4, it was assumed that it does not matter to which governing equations forcing is applied, as long as the forcing occurs gradually over a thick enough zone. The present findings implicate though, that predictions may be less accurate when applying forcing to a governing equation which has a negligible contribution to the overall wave energy (for a wave with period $T = T_\mathrm{peak}$, the vertical kinetic energy is only $E_{\mathrm{kin},z} \approx 0.006 E_{\mathrm{kin},x}$, i.e. roughly 0.3% of the total wave energy). In spite of the slight decrease in accuracy for parameter settings far from the optimum values, for close-to-optimum forcing the theory predictions and simulation results agree reasonably well as before.

Additionally, the simulations from Figs. 8 to 10 were repeated with forcing of velocities u and w as well as volume fraction α towards the calm-surface solution. The theory predictions for optimum γ-values provide satisfactory reduction of undesired wave reflections, and tuning the forcing zone to the peak wave period T_peak again predicts these settings reasonably well.

As with regular waves, Figs. 15 to 17 show that reflection is over-predicted by theory for larger-than-optimum values of γ. In contrast to deep-water conditions, the range for satisfactory reduction of undesired reflections (say $C_\mathrm{R} < 5\%$) is significantly wider and extends onto several orders of magnitude larger values of forcing strengths γ than theoretically expected. Comparison of Figs. 8 and 11 (bottom, right) shows that for too strong forcing in shallow water, forcing of x-momentum in contrast to forcing of volume fraction α reflect the waves with similar reflection coefficients but with *inverted surface elevation* as explained in the caption of Fig. 11. The reason for the low reflection coefficients for theoretically too-strong forcing in Figs. 15 to 17 is therefore the cancellation of the waves reflected due to forcing of x-momentum and due to forcing of volume fraction α.

Finally, repeating the simulations with x-momentum forcing with a thicker forcing zone ($x_\mathrm{d} = 2\lambda_\mathrm{peak}$) in Figs. 18 to 20 shows that the range of γ-values which provide satisfactory reduction of undesired wave reflections widens and the reflection coefficient C_R at optimum tuning decreases. As

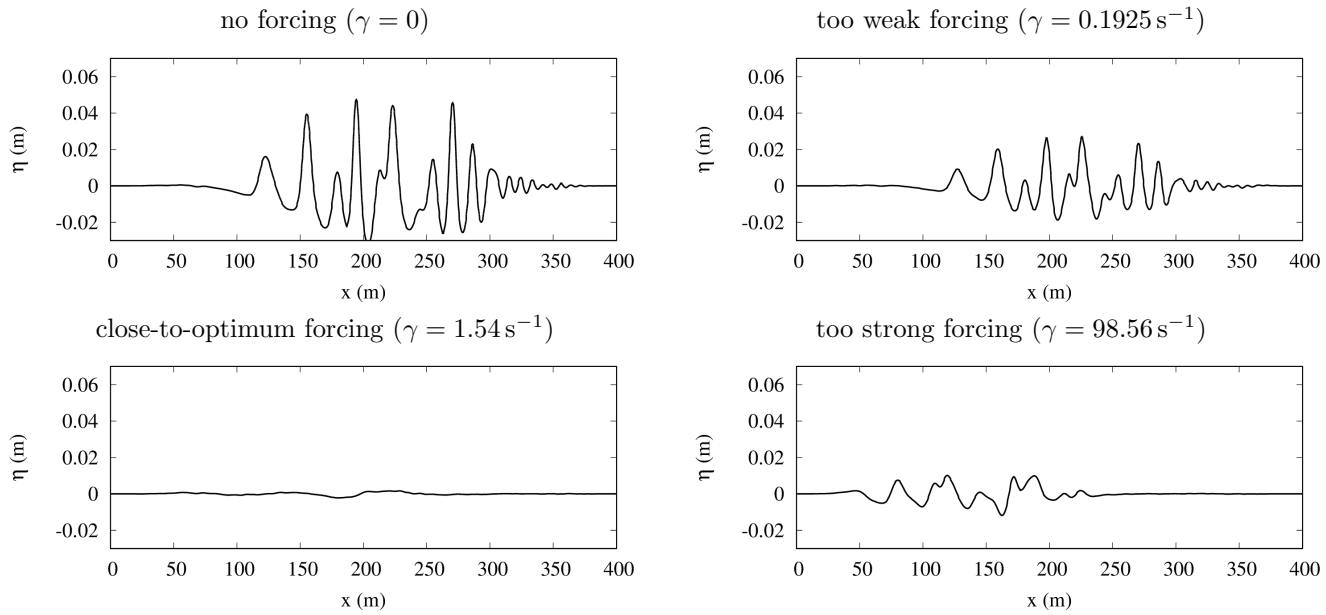

Figure 11: As Fig. 8, except for forcing of volume fraction α; note that for too strong forcing ($\gamma = 98.56\,\mathrm{s}^{-1}$), the surface elevation looks like the inverted corresponding plot from Fig. 8, meaning that all wave troughs from Fig. 8 are peaks in Fig. 11 and all peaks are troughs; this explains why forcing of both x-momentum and volume fraction α in Fig. 15 produces low reflection coefficients even for substantially stronger than optimum forcing, since the wave components reflected due to forcing of x-momentum and volume fraction α cancel

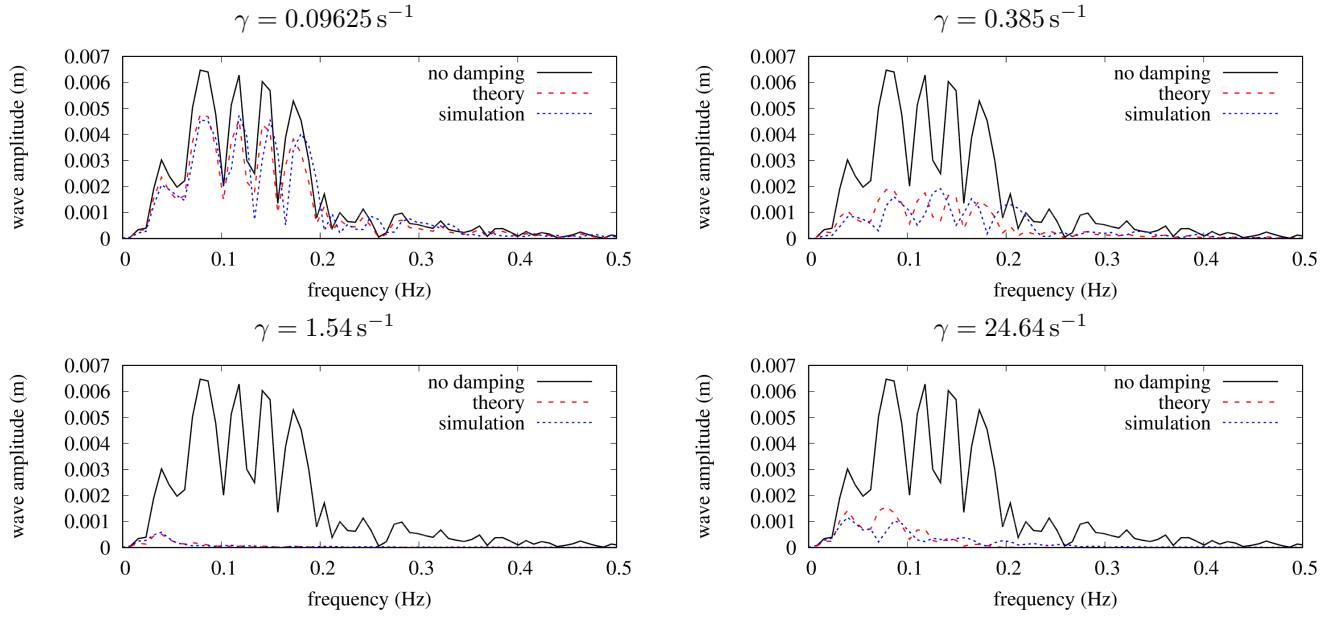

Figure 12: As Fig. 9, except for forcing of volume fraction α

before, the theory predicts the simulation results reasonably well, though reflection coefficients at close-to-optimum setting are slightly under-predicted. Thus it is recommended to use slightly thicker forcing zones than theory may suggest to ensure reliable damping. As before, tuning the forcing zone to the peak period detects the optimum choice of forcing strength γ reasonably well, although it underpredicts the corresponding reflection coefficients C_R more strongly than the theory for the overall reflection coefficient.

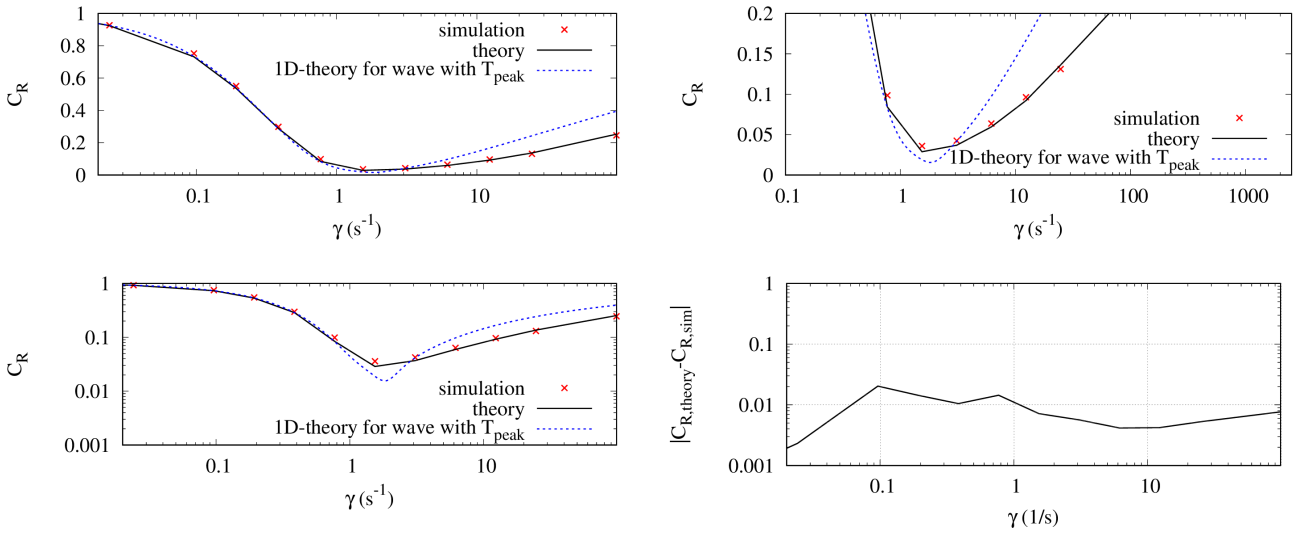

Figure 13: As Fig. 10, except for forcing of volume fraction α; for all simulation results $C_{\mathrm{R,sim}}$ and corresponding theory predictions $C_{\mathrm{R,theory}}$ holds $C_{\mathrm{R,sim}} - C_{\mathrm{R,theory}} < 2.1\%$ and on average $|C_{\mathrm{R,sim}} - C_{\mathrm{R,theory}}| < 0.6\%$; for the forcing strength $\gamma \geq \gamma_{\mathrm{opt,theory}}$ closest to the theoretical optimum value $\gamma_{\mathrm{opt,theory}}$ holds $C_{\mathrm{R,sim}} - C_{\mathrm{R,theory}} < 0.8\%$

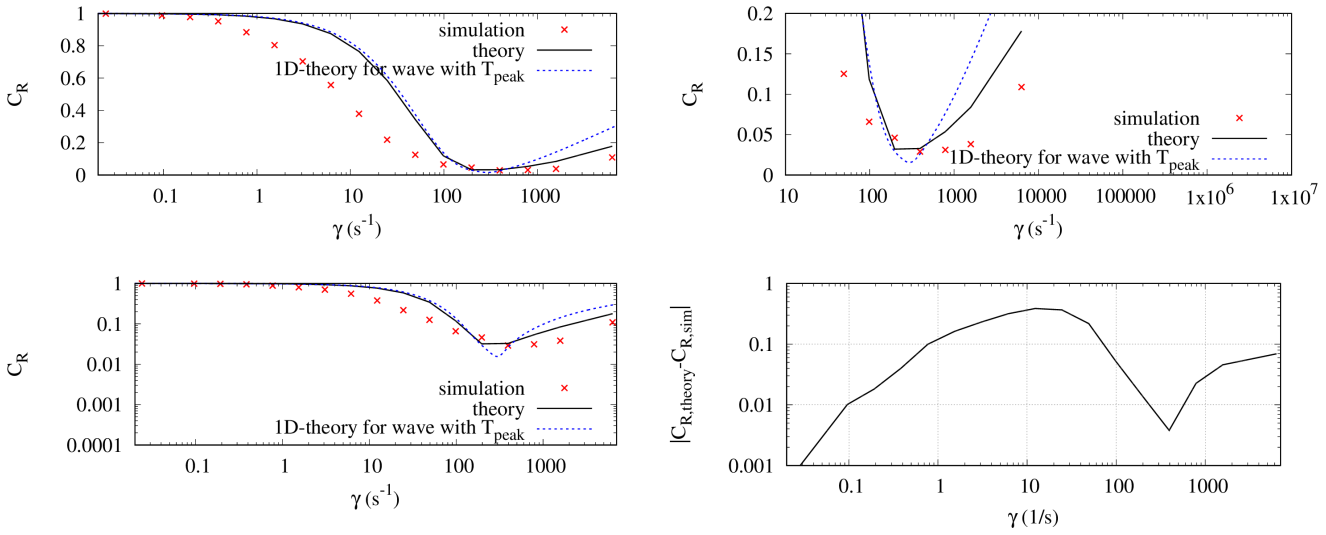

Figure 14: As Fig. 10, except for forcing of z-momentum; for all simulation results $C_{\mathrm{R,sim}}$ and corresponding theory predictions $C_{\mathrm{R,theory}}$ holds $C_{\mathrm{R,sim}} - C_{\mathrm{R,theory}} < 1.5\%$; for the forcing strength $\gamma \geq \gamma_{\mathrm{opt,theory}}$ closest to the theoretical optimum value $\gamma_{\mathrm{opt,theory}}$ holds $C_{\mathrm{R,sim}} - C_{\mathrm{R,theory}} < 1.5\%$

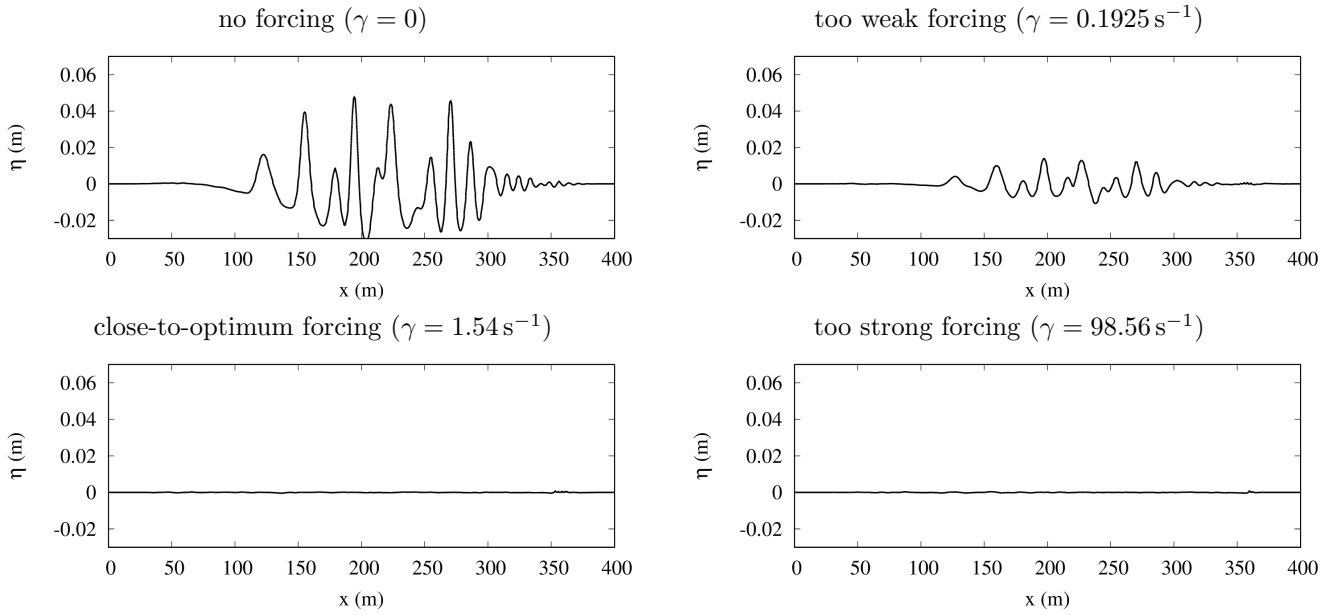

Figure 15: As Fig. 8, except for forcing of x- and z-momentum and volume fraction α

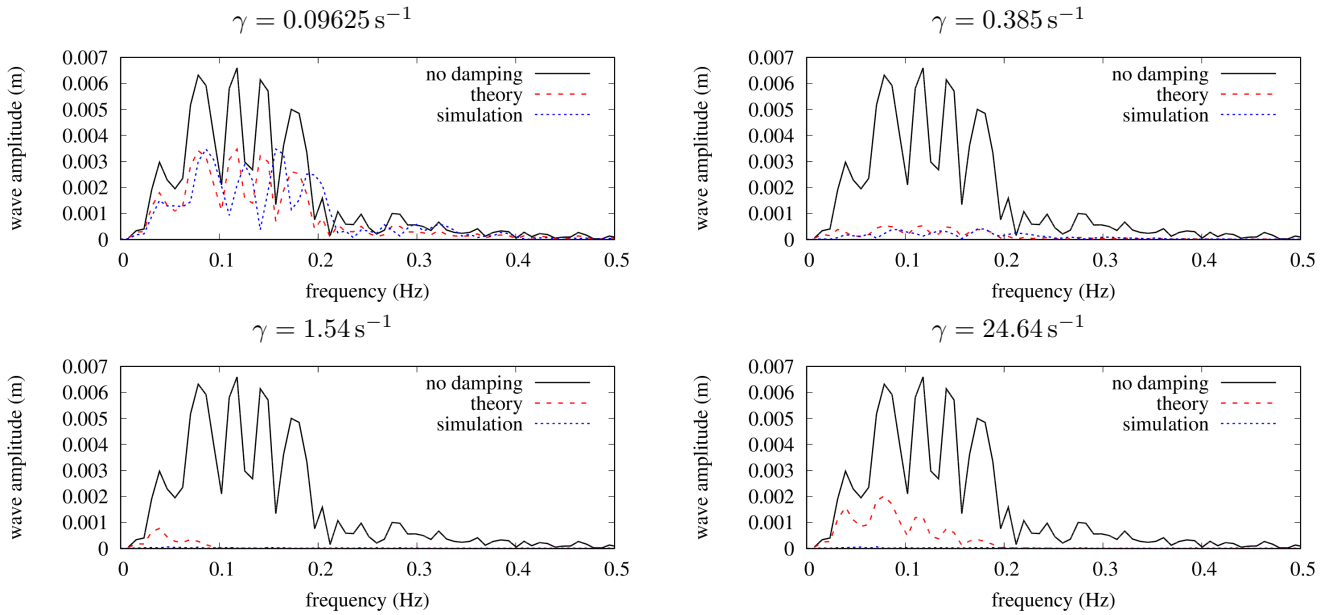

Figure 16: As Fig. 9, except for forcing of x- and z-momentum and volume fraction α

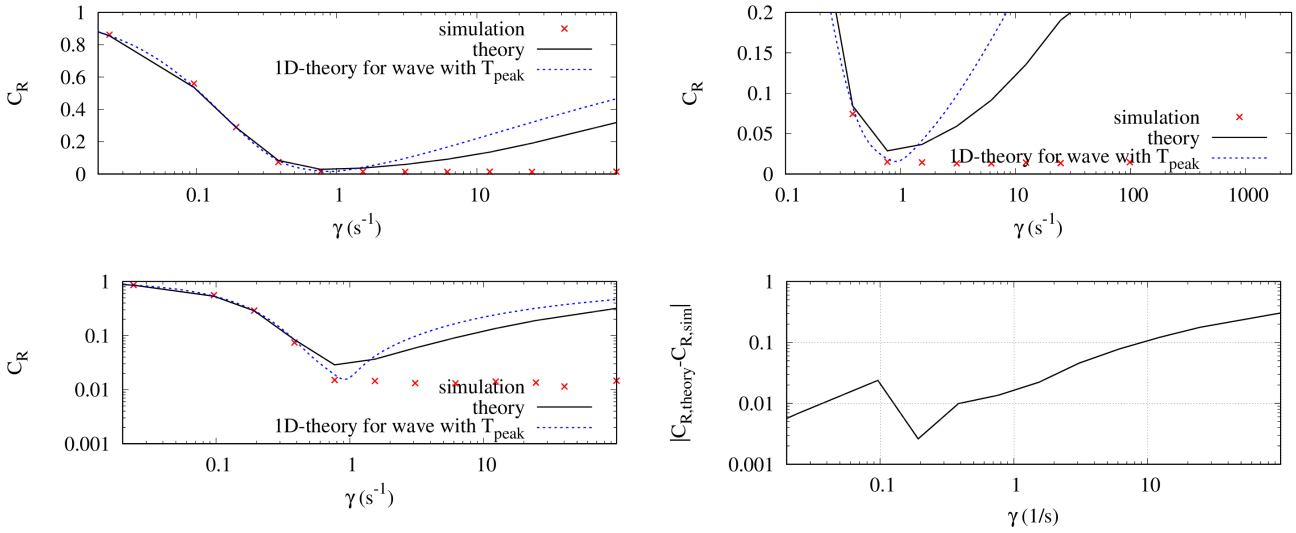

Figure 17: As Fig. 10, except for forcing of x- and z-momentum and volume fraction α; for all simulation results $C_{\mathrm{R,sim}}$ and corresponding theory predictions $C_{\mathrm{R,theory}}$ holds $C_{\mathrm{R,sim}} - C_{\mathrm{R,theory}} < 2.4\%$; for the forcing strength $\gamma \geq \gamma_{\mathrm{opt,theory}}$ closest to the theoretical optimum value $\gamma_{\mathrm{opt,theory}}$ holds $C_{\mathrm{R,sim}} - C_{\mathrm{R,theory}} < -1.3\%$

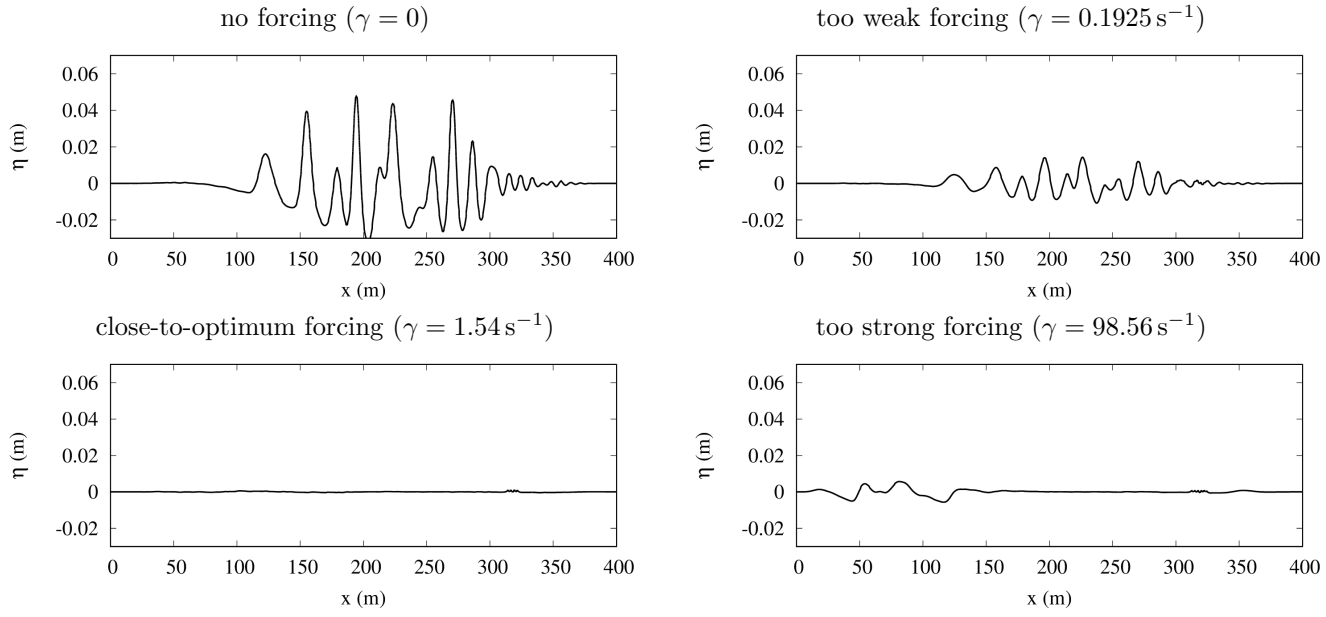

Figure 18: As Fig. 8, except for zone thickness $x_{\mathrm{d}} = 2\lambda_{\mathrm{peak}}$

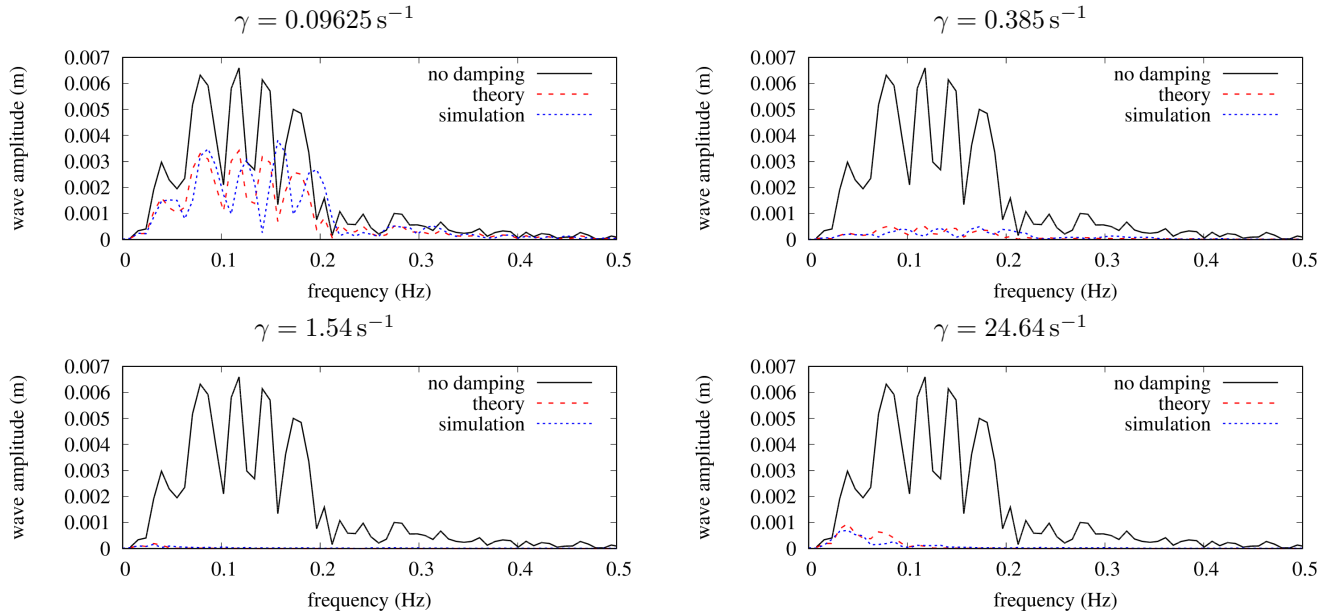

Figure 19: As Fig. 9, except for zone thickness $x_\mathrm{d} = 2\lambda_\mathrm{peak}$

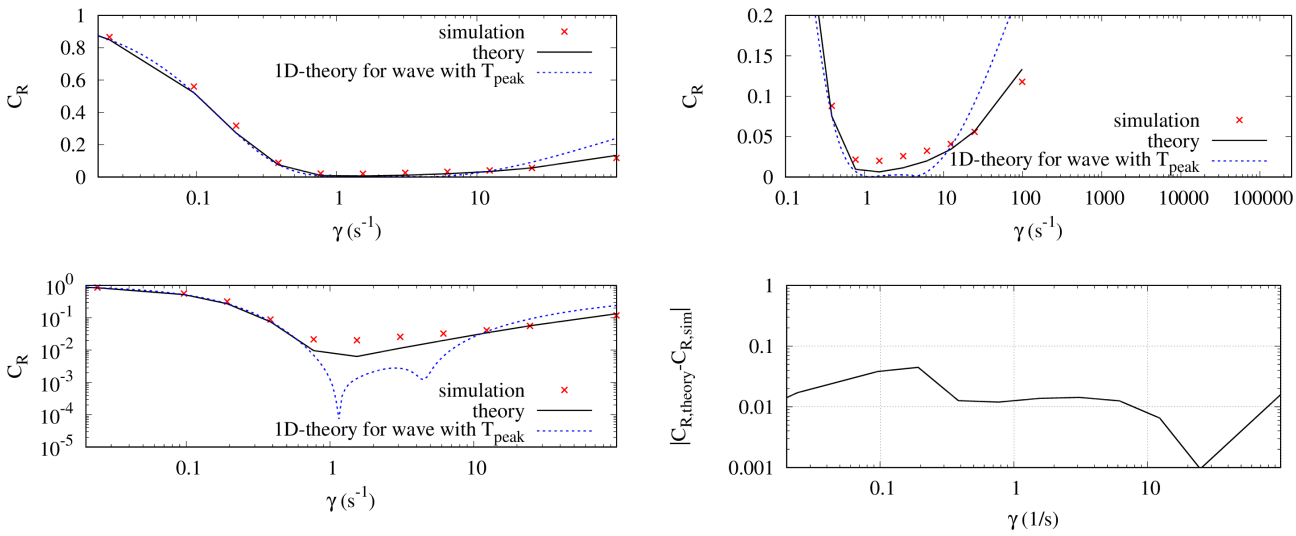

Figure 20: As Fig. 10, except for zone thickness $x_\mathrm{d} = 2\lambda_\mathrm{peak}$; for all simulation results $C_\mathrm{R,sim}$ and corresponding theory predictions $C_\mathrm{R,theory}$ holds $C_\mathrm{R,sim} - C_\mathrm{R,theory} < 4.5\%$ and on average $|C_\mathrm{R,sim} - C_\mathrm{R,theory}| < 1.3\%$; for the forcing strength $\gamma \geq \gamma_\mathrm{opt,theory}$ closest to the theoretical optimum value $\gamma_\mathrm{opt,theory}$ holds $C_\mathrm{R,sim} - C_\mathrm{R,theory} < 1.4\%$

8 DISCUSSION

The results from Sect. 6 demonstrate that the theory from Sect. 4 satisfactorily predicts reflection coefficients C_R of forcing zones for highly non-linear free-surface waves. It was found that the wave's non-linearity had no significant influence on the accuracy of the theory's predictions. Since the theory was derived based on linear wave theory, the question arises how can its predictions be so accurate also for highly non-linear waves?

This question can be answered based on the findings from Sects. 4 and 6, which show that forcing zones reduce undesired wave reflections via three mechanisms: wave absorption, partial wave reflection occurring throughout the zone (cf. Figs. 2 and 5), and destructive interference of these partial wave reflections (cf. Fig. 11).

Figure 5 illustrates that when a forcing zone is optimally tuned, then the wave envelope gradually decreases throughout the forcing zone and partial wave reflections occur throughout the whole forcing zone with small amplitude; thus forcing zones 'split up' non-linear waves into many approximately linear wave components, which interfere destructively due to their phase differences.

This behavior characterizes a key difference between forcing zone approaches and boundary-based wave absorption techniques such as absorbing boundary conditions (see e.g. Colonius, 2004; Givoli, 2004) or active wave absorption (e.g. Cruz, 2008; Schäffer and Klopman, 2000): Boundary-based approaches can neither utilize partial wave reflections nor their destructive interference, since they act only at the boundary. This explains why forcing zones, despite their simple formulation, are capable of damping even highly non-linear waves in complex flow problems, where high-order boundary-based wave damping approaches would fail.

The results from Sect. 7 show that the theory from Sect. 4 satisfactorily predicts the reflected wave amplitude spectrum as well as the overall reflection coefficient C_R for irregular waves.

Further, it was found that already tuning the forcing zone based on the peak period T_peak of the investigated wave energy spectrum provided a decent estimate of the optimum values for the case-dependent parameters of the forcing zone. With this simplified approach, the theory slightly underpredicted the corresponding reflection coefficient C_R. However, this is not considered a serious drawback, since for engineering practice it is recommended to select the forcing zone thickness x_d slightly thicker than theoretically necessary to ensure satisfactory reduction of undesired wave reflections. Thus also the simplified approach for tuning forcing zones for irregular waves is recommended for practical use.

Although this work presented results from 2D-flow simulations, the results are expected to also apply to 3D-flow simulations with forcing zones. This assessment is based on published results for 3D-flow simulations with strongly reflecting bodies subjected to non-linear waves (cf. Perić et al., 2018, wave steepness ca. 71% of breaking steepness; Perić and Abdel-Maksoud, 2019, wave steepness ca. 36% of breaking steepness) and irregular waves (cf. Perić and Abdel-Maksoud, 2019), where the theory from Sect. 4 was found to provide satisfactory tuning of the forcing zone's parameters. The present results help to explain the findings from these works and provide insight into the mechanisms behind how forcing zones reduce undesired wave reflections. Further research is in progress to provide a deeper understanding of the applicability of the present findings to 3D-flow simulations with forcing zones.

9 CONCLUSION

In this work, 2D-flow simulations with free-surface waves were performed for non-linear deep-water waves with steepness up to 85% of the breaking steepness and for irregular waves in close to shallow-water depth. Forcing zones were used to minimize undesired wave reflections at the domain boundaries. Different values for the case-depenendent parameters of the forcing zones were investigated and the resulting wave reflection coefficients were compared with theory predictions. The wave's non-linearity was found to have a negligible influence on the forcing zone's reflection coefficient C_R. Two approaches have been presented for tuning the forcing zone parameters in investigations with irregular waves. Based on the discussion in Sect. 8, the present findings are expected to apply also to 3D-flow simulations.

When the forcing zone was tuned using the theory from Sect. 4, the simulation results for reflection coefficient C_R were in most cases smaller or nearly equal to those predicted by theory, but never more than 2.1% larger. Therefore the theory is recommended for tuning forcing zones in flow simulations with non-linear and irregular free-surface waves.

ACKNOWLEDGEMENTS

The authors gratefully acknowledge the financial support by grant AB 112/11-1 by the Deutsche Forschungsgemeinschaft (DFG) for this study.

REFERENCES

[1] Chen, H. C., Yu, K., & Chen, S. Y. (2006). Simulation of Wave Runup Around Offshore Structures by a Chimera Domain Decomposition Approach. In Civil Engineering in the Oceans VI (pp. 267-280).

[2] Choi, J., & Yoon, S. B. (2009). Numerical simulations using momentum source wave-maker applied to RANS equation model. Coastal Engineering, 56(10), 1043-1060.

[3] Colonius, T. (2004). Modeling artificial boundary conditions for compressible flow. Annu. Rev. Fluid Mech., 36, 315-345.

[4] Cruz, J. (ed.) (2008). Ocean wave energy: current status and future prespectives. Springer Series in Green Energy and Technology, Berlin.

[5] DNV (DET NORSKE VERITAS AS) (2014). Environmental conditions and environmental loads. Link (accessed 15 March 2018): `http://rules.dnvgl.com/docs/pdf/DNV/codes/docs/2014-04/RP-C205.pdf`

[6] Fenton, J. D. (1985). A fifth-order Stokes theory for steady waves. Journal of waterway, port, coastal, and ocean engineering, 111(2), 216-234.

[7] Ferziger, J. H., & Peric, M. (2002). Computational methods for fluid dynamics. Springer Science & Business Media.

[8] Givoli, D. (2004). High-order local non-reflecting boundary conditions: a review. Wave motion, 39(4), 319-326.

[9] Hasselmann, K., Barnett, T.P., Bouws, E., Carlson, H., Cartwright, D.E., Enke, K., Ewing, J.A., Gienapp, H., Hasselmann, D.E., Kruseman, P. & Meerburg, A. (1973). Measurements of wind-wave growth and swell decay during the Joint North Sea Wave Project (JONSWAP). Ergänzungsheft 8-12.

[10] Israeli, M., & Orszag, S. A. (1981). Approximation of radiation boundary conditions. Journal of computational physics, 41(1), 115-135.

[11] Jacobsen, N. G., Fuhrman, D. R., & Fredsøe, J. (2012). A wave generation toolbox for the open-source CFD library: OpenFoam®. International Journal for Numerical Methods in Fluids, 70(9), 1073-1088.

[12] Kim, J., O'Sullivan, J., & Read, A. (2012). Ringing analysis of a vertical cylinder by Euler overlay method. In ASME 2012 31st International Conference on Ocean, Offshore and Arctic Engineering (pp. 855-866). American Society of Mechanical Engineers.

[13] Mayer, S., Garapon, A., & Sørensen, L. S. (1998). A fractional step method for unsteady free-surface flow with applications to non-linear wave dynamics. International Journal for Numerical Methods in Fluids, 28(2), 293-315.

[14] Michell, J. H. (1893). XLIV. The highest waves in water. The London, Edinburgh, and Dublin Philosophical Magazine and Journal of Science, 36(222), 430-437.

[15] Muzaferija, S., & Perić, M. (1999). Computation of free surface flows using interface-tracking and interface-capturing methods. In Mahrenholtz, O., Markiewicz, M. (Eds.), Nonlinear Water Wave Interaction (pp. 59-100). WIT Press, Southampton.

[16] Park, J. C., Kim, M. H., & Miyata, H. (1999). Fully non-linear free-surface simulations by a 3D viscous numerical wave tank. International Journal for Numerical Methods in Fluids, 29(6), 685-703.

[17] Perić, R., & Abdel-Maksoud, M. (2016). Reliable damping of free-surface waves in numerical simulations. Ship Technology Research, 63(1), 1-13.

[18] Perić, R., & Abdel-Maksoud, M. (2018). Analytical prediction of reflection coefficients for wave absorbing layers in flow simulations of regular free-surface waves. Ocean Engineering, 147, 132-147.

[19] Perić, R., Abdel-Maksoud, M. (2019). Reducing Undesired Wave Reflection at Domain Boundaries in 3D Finite Volume–Based Flow Simulations via Forcing Zones. Journal of Ship Research, 63.

[20] Perić, R., Vukčević, V., Abdel-Maksoud, M., & Jasak, H. (2018). Tuning the case-dependent parameters of relaxation zones for flow simulations with strongly reflecting bodies in free-surface waves. arXiv preprint arXiv:1806.10995.

[21] Schäffer, H. A., & Klopman, G. (2000). Review of multidirectional active wave absorption methods. Journal of waterway, port, coastal, and ocean engineering, 126(2), 88-97.

[22] Ursell, F., Dean, R. G., & Yu, Y. S. (1960). Forced small-amplitude water waves: a comparison of theory and experiment. Journal of Fluid Mechanics, 7(1), 33-52.

[23] Vukčević, V., Jasak, H., & Malenica, Š. (2016a). Decomposition model for naval hydrodynamic applications, Part I: Computational method. Ocean Engineering, 121, 37-46.

[24] Vukčević, V., Jasak, H., & Malenica, Š. (2016b). Decomposition model for naval hydrodynamic applications, Part II: Verification and validation. Ocean engineering, 121, 76-88.